Environmental Science & Technology

pubs.acs.org/est

Article

Star Polymer Size, Charge Content, and Hydrophobicity Affect their Leaf Uptake and Translocation in Plants

Yilin Zhang, Liye Fu, Sipei Li, Jiajun Yan, Mingkang Sun, Juan Pablo Giraldo, Krzysztof Matyjaszewski, Robert D. Tilton,* and Gregory V. Lowry*

Cite This: *Environ. Sci. Technol.* 2021, 55, 10758−10768

Read Online

ACCESS | Metrics & More | Article Recommendations | Supporting Information

ABSTRACT: Determination of how the properties of nanocarriers of agrochemicals affect their uptake and translocation in plants would enable more efficient agent delivery. Here, we synthesized star polymer nanocarriers poly(acrylic acid)-*block*-poly(2-(methylsulfinyl)ethyl acrylate) (PAA-*b*-PMSEA) and poly(acrylic acid)-*block*-poly((2-(methylsulfinyl)ethyl acrylate)-*co*-(2-(methylthio)ethyl acrylate)) (PAA-*b*-P(MSEA-*co*-MTEA)) with well-controlled sizes (from 6 to 35 nm), negative charge content (from 17% to 83% PAA), and hydrophobicity and quantified their leaf uptake, phloem loading, and distribution in tomato (*Solanum lycopersicum*) plants 3 days after foliar application of 20 μL of a 1g L^{-1} star polymer solution. In spite of their property differences, ∼30% of the applied star polymers translocated to other plant organs, higher than uptake of conventional foliar applied agrochemicals (<5%). The property differences affected their distribution in the plant. The ∼6 nm star polymers exhibited 3 times higher transport to younger leaves than larger ones, while the ∼35 nm star polymer had over 2 times higher transport to roots than smaller ones, suggesting small star polymers favor symplastic unloading in young leaves, while larger polymers favor apoplastic unloading in roots. For the same sized star polymer, a smaller negative charge content (yielding $\zeta \sim -12$ mV) enhanced translocation to young leaves and roots, whereas a larger negative charge ($\zeta < -26$ mV) had lower mobility. Hydrophobicity only affected leaf uptake pathways, but not translocation. This study can help design agrochemical nanocarriers for efficient foliar uptake and targeting to desired plant organs, which may decrease agrochemical use and environmental impacts of agriculture.

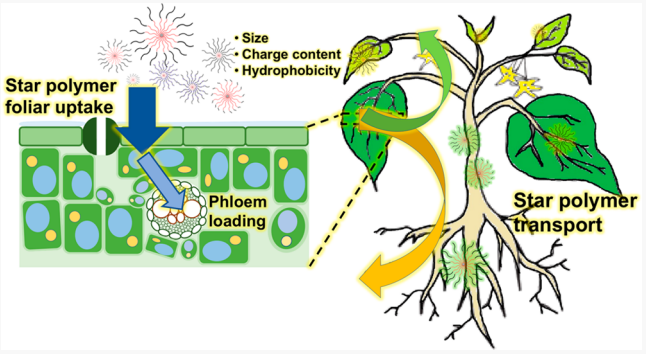

KEYWORDS: *star polymer, agent delivery, phloem loading, foliar application, agrochemicals*

1. INTRODUCTION

Agrochemical application is inefficient, with low uptake of active ingredients (<0.1%) and micronutrients (<5%) leading to unsustainable environmental impacts.[1−4] The majority of the soil and foliar sprayed conventional agrochemicals (typically metal ions and small organic molecules) are lost through infiltration or runoff, degrading environmental quality.[5,6] New approaches that deliver agrochemicals more efficiently are needed to reduce agrochemical application rates, hence lowering the environmental impact from agriculture.

Nanoparticle (NP) foliar application could be a potential solution to improve agrochemical application efficiency.[3,7−10] NPs with different size and charge applied to both monocot and dicot plants have shown significant uptake through foliar pathways.[3,11−14] After nearly 100% of applied Au NPs were taken up into wheat leaves over a few days, up to 60% of those AuNPs transported to other plant compartments in wheat plants.[3] Star polymers (polymer NPs) and liposome based nanocarriers are also efficiently taken up and translocated in tomato plants after foliar application. These carriers have also demonstrated controlled *in vivo* agent delivery.[2,15] The potential for higher plant uptake and transport achieved by NP foliar applications compared to that of conventional agrochemical application such as soil applications and direct foliar spray of active ingredients make it a promising approach for reducing use of agrochemicals and delivering agrochemicals into desired plant compartments more efficiently.[3,11,16,17]

The factors affecting NP uptake and their systemic translocation pathways in plants remain unclear, and this prevents their delivery in a controlled and targeted manner.[3] NPs can enter plant leaves through two major paths: stomata infiltration and cuticle penetration (see Scheme 1a). The NP surface properties are known to play a role in foliar uptake.[3]

Received: February 14, 2021
Revised: May 14, 2021
Accepted: July 6, 2021
Published: July 20, 2021

Scheme 1. Plant Leaf Pathways and Potential Barriers during Phloem Transport

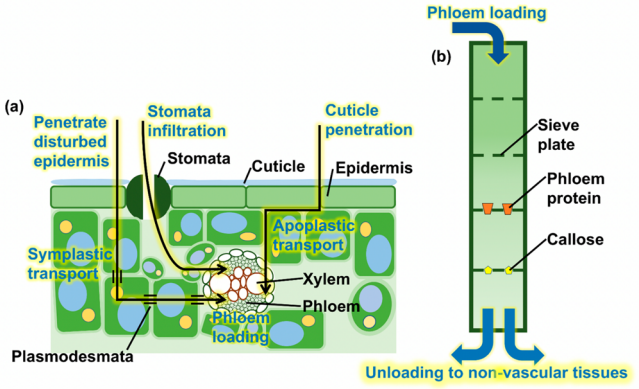

(a) Plant leaf pathways of star polymer cell uptake and phloem loading, and related plant organs, including cuticle, epidermis, stomata, cell wall, and cell plasmodesmata. Star polymers enter the leaf epidermis through stomatal pores, cuticle layer or disrupted epidermal cells. Transport processes for phloem loading through apoplastic and symplastic transport. (b) Potential barriers during phloem transport include sieve plates, phloem P protein and callose plugs that are produced as a response to phloem pathogens or injury.

The more hydrophobic polyvinylpyrrolidone (PVP) and hydrophilic citrate coated AuNPs can interact with cuticle differently. The PVP coated AuNPs were translocated through the cuticle more than the citrate coated AuNPs.[3] The monocot and dicot plants, with different leaf anatomy, will experience NP foliar uptake differently due to differences in stomata density and mesophyll cell packing density,[11] as the monocot maize plants were found to take up NPs mainly through the stomata pathway, while the dicot cotton plants take up NPs through both stomata and cuticle pathways.[11] While transcuticular pathways are being explored, almost nothing is known about how NP properties affect transport through the leaf mesophyll into the vasculature, i.e., phloem and xylem.[3] After crossing the cuticle and epidermis, NPs may move through mesophyll by either symplastic (within cells and through plasmodesmata)[18] or apoplastic transport (through the extracellular space) to reach the phloem and be further transported from the exposed leaves to other plant organs (Scheme 1a). Phloem transports photosynthates (sugars) from photosynthetic organelles in mature leaves to younger leaves and roots.[19] After being loaded into phloem, NP transport could still be regulated by sieve plates, callose, and phloem proteins produced during plant immune responses (Scheme 1b).[20−22] To reach other nonvascular plant organs other than the dosed leaf, the NPs also first must go through the vasculature in the stem. While being transported in phloem, NPs could also be exchanged from the phloem to the xylem, depending on the vascular structure of the plants and the properties of NPs.[23,24] Finally, the NP unloading from phloem into other nonvascular tissue may also influence their distribution in plants.[25]

NP physical and chemical properties can affect their interactions with different plant organelles and influence their transport behavior in plants.[26,27] Systems have been studied where NPs having a size and net charge above critical values can penetrate cell membranes, enabling their entrance into mesophyll cells and chloroplasts.[11,26] However, sizes exceeding a certain range could also inhibit NP colocalization with plant cells.[11] Besides net charge, the sign of charge also affects NP affinity to different organelles, as negatively charged nanoceria delivered by needless syringe infiltration in buffer have shown higher colocalization with *Arabidopsis thaliana* chloroplasts than positively charged counterparts.[7] However, positively charged NPs delivered by topical foliar application in surfactants are more efficiently delivered to chloroplasts in maize and cotton than their negatively charged counterparts.[11] The physical and chemical properties of polymer carriers, including size, charge, and hydrophobicity, could therefore all play important roles deciding their uptake, transport, and biodistribution in plants organs after foliar exposure.

Polymer based nanocarriers are emerging materials for more efficient agrochemical delivery in plants.[28] New materials, including star polymers, have been developed for agent delivery and plant stress management through targeted delivery approaches.[2,7,16] However, targeted delivery of these new polymer based nanocarriers into desired plant compartments is challenging because the properties affecting star polymer (nanocarrier) uptake and transport in plants have not yet been investigated. Star polymers consist of multiple polymer chain "arms" emanating from a central core. Since the arms of soluble star polymers are swollen with solvent, they are soft materials. As such, they may interact with plant compartments differently compared to rigid metal or metal oxide NPs. The general trends now emerging from metal/metal oxide NP-plant interaction studies may not be applicable for star polymers. In this study, PAA-*b*-PMSEA and PAA-*b*-P(MSEA-*co*-MTEA) star polymers with well-controlled sizes (6−35 nm, determined by degree of polymerization of their arms), negative charge content (determined by the charged AA monomer content) and hydrophobicity (determined by MSEA:MTEA ratio) were synthesized by atom transfer radical polymerization (ATRP).[29] The total transport (phloem loading) efficiency and biodistribution of foliar applied star polymers in tomato plants were assessed by inductively coupled plasma mass spectrometry (ICP-MS). The route of uptake and interaction between star polymers and tomato leaves with or without surfactants was studied by Hyperspectral-Enhanced Dark Field Microscopy (DF-HSI). These studies revealed that the star polymer properties affected the delivery location, but not overall uptake efficiency.

2. EXPERIMENTAL SECTION

Materials. 2-(Methylthio)ethanol (≥99%), hydrogen peroxide solution (30% H_2O_2, ACS grade), tris[2-(dimethylamino)ethyl]amine (Me_6Tren), anisole (99%), *N*,*N*-dimethylformamide (DMF, 99%), trifluoroacetic acid (TFA, 99%), gadolinium(III) chloride hexahydrate ($GdCl_3 \cdot 6H_2O$, 99%), and HNO_3 (70%, trace metal grade) were purchased from Fisher Scientific. Acrylic acid (≥99%), *tert*-butyl acrylate (≥99%), *N*-(3-(dimethyl amino)propyl)-*N*′-ethylcarbodiimide hydrochloride (EDC, ≥99%), *N*,*N*-dimethyl aminopyridine (DMAP, ≥99%), copper bromide (≥99.99%), *β*-cyclodextrin (*β*-CD), 2-bromoisobutyryl bromide (BiBB, 98%), 1-methyl-2-pyrrolidone (NMP), methanol (99.8%), dichloromethane (DCM), sodium persulfate (≥98%), sodium sulfate (≥99%), crystal violet (CV, >90%), and chloroform-*d* ($CDCl_3$) were purchased from Sigma-Aldrich. Dialysis bags with various molecular weight cutoffs (Spectra/Por 7) were purchased from Spectrum Chemical Manufacturing Corp. Silwet L-77 surfactant was purchased from PhytoTech laboratories, Inc. Tomato seeds (Roma VF) were purchased

https://doi.org/10.1021/acs.est.1c01065
Environ. Sci. Technol. 2021, 55, 10758−10768

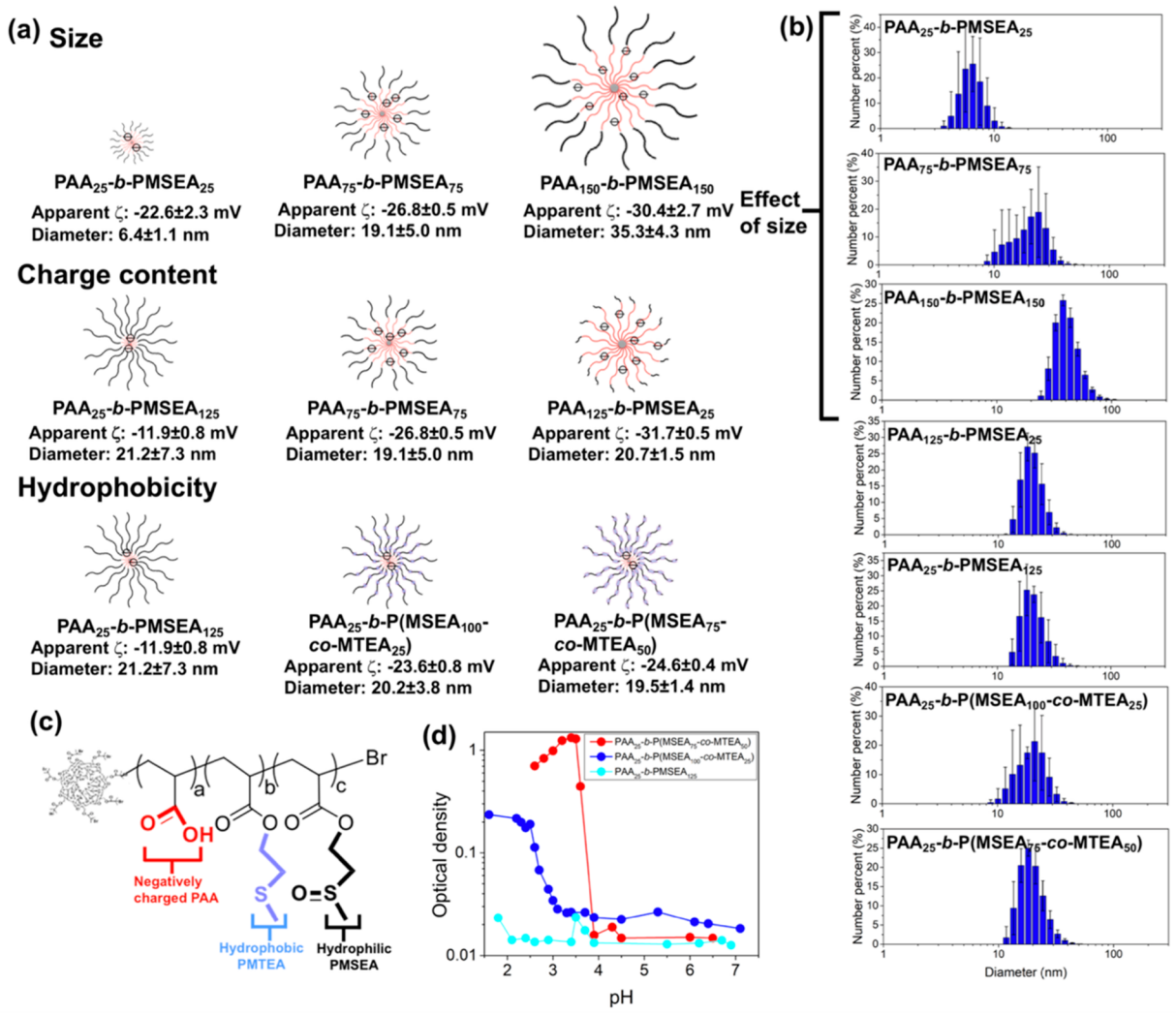

Figure 1. (a) Different physical and chemical properties of star polymers investigated in this study. Size is adjusted by changing total DP of each arm, charge content is adjusted by varying the PAA (negatively charged) to PMSEA (neutral) molar ratio, and star polymer hydrophobicity is adjusted by copolymerizing hydrophilic MSEA with hydrophobic MTEA in the outer block of star polymer arms. (b) Number-average diameter distribution of PAA-*b*-PMSEA and PAA-*b*-P(MSEA-*co*-MTEA) star polymers. Hydrodynamic diameters were determined in water at 100 mg L^{-1} star polymer concentration at pH 6.5 (10 mM NaCl) by dynamic light scattering (Malvern zetasizer nano zs). The electrophoretic mobility was measured in the same solutions (pH = 6.5, 10 mM NaCl) using the Malvern zetasizer nano zs. Apparent zeta potentials (ζ) were calculated from the mobility via the Smoluchowski model. (c) Schematic illustration of the chemical composition of PAA-*b*-P(MSEA-*co*-MTEA) star polymer arms and chemical properties of different repeating units. (d) Optical density at 541 nm vs pH for PAA_{25}-*b*-$PMSEA_{125}$, PAA_{25}-*b*-P($MSEA_{100}$-*co*-$MTEA_{25}$), and PAA_{25}-*b*-P($MSEA_{75}$-*co*-$MTEA_{50}$) star polymers. Increased optical density indicates star polymer aggregation driven by hydrophobicity.

from Atlee Burpee & Co. Acrylate monomers were passed through a basic alumina column before use. Water was purified by Milli-Q IQ 7000 lab water system. Other chemicals were used without further purification.

Synthesis of MTEA and MSEA Monomers. *Synthesis of 2-(Methylthio)ethyl Acrylate (MTEA).* The MTEA was synthesized according to a previously published procedure.[29,30] Briefly, acrylic acid (8.6 g, 1.1 equiv), *N*-(3-(dimethylamino)-propyl)-*N*′-ethylcarbodiimide hydrochloride (EDC·HCl, 24 g, 1.15 equiv), and 4-dimethylaminopyridine (DMAP, 1.89 g, 0.14 equiv) were dissolved into 200 mL of dichloromethane (DCM) in a 500 mL round-bottom flask equipped with a stir bar in ice bath. The reactor was sealed and purged with N_2 for 10 min. Then, 2-(methylthio)ethanol (10 g, 1.0 equiv) was injected into the reactor. The reaction proceeded at room temperature for 24 h, and reagent conversion was monitored by proton nuclear magnetic resonance (^{1}H NMR, Bruker 500 MHz NMR spectrometers). The product in DCM was washed by 0.1 M HCl (2x, 150 mL), followed by washing with saturated $NaHCO_3$ (2x, 150 mL) to remove residual reagents and washing by brine (1x, 150 mL); this was followed by the addition of anhydrous Na_2SO_4 to remove residual water. DCM was removed by rotary evaporator (Buchi V-850). The purity of MTEA was confirmed by ^{1}H NMR (Figure S1a).

Synthesis of 2-(Methylsulfinyl)ethyl Acrylate (MSEA). The MSEA was synthesized by oxidizing MTEA according to a previous provedure.[29,30] A 5 g portion of MTEA was added into a glass vial sealed by a rubber stopper and equipped with a magnetic stir bar. The vial was kept in an ice bath and purged by N_2 for 5 min to remove water and oxygen. A 3.8 g portion of a 30% H_2O_2 solution was slowly added to MTEA by a syringe pump at 50 μL min^{-1}. The reaction proceeded for 24 h

https://doi.org/10.1021/acs.est.1c01065
Environ. Sci. Technol. 2021, 55, 10758−10768

and was stopped by the additio of 50 mL of Milli-Q water. The MSEA in water was extracted three times into 100 mL of DCM and passed through a column filled with 50 wt % anhydrous Na_2SO_4 and 50 wt % $Na_2S_2O_8$ to remove water and H_2O_2. Excess solvent was removed by rotary evaporator to yield MSEA. The purity of MSEA is confirmed by ^{1}H NMR (Figure S1b).

Synthesis of 21-Arm PAA-b-PMSEA and PAA-b-P(MSEA-co-MTEA) Star Polymers with Different Size, Charge Content, and Hydrophobicity. The PAA-*b*-PMSEA and PAA-*b*-P(MSEA-*co*-MTEA) star polymers with different size, charge content, and shell hydrophobicity were made by a core-first approach.[2,31] *β*-Cyclodextrin was first functionalized with 2-bromoisobutyryl bromide (BiBB) to yield an ATRP macroinitiator with 21 initiating sites (*β*-CD-21Br). The *β*-CD-21Br was then used to initiate ATRP of *t*BA, to make a 21-arm P*t*BA star polymer, with either 25, 75, 125, or 150 degree of polymerization (DP) in each arm. The arms in P*t*BA star polymers were then extended with different ratios of MSEA and MTEA to produce P*t*BA-*b*-PMSEA or P*t*BA-*b*-P(MSEA-*co*-MTEA) star polymers. The chemical composition of the star polymers were assessed by ^{1}H NMR, and their dispersity was assessed by gel permeation chromatography (GPC).[2] Star polymers with different size but similar compositions were made by varying the total DP in each arm from 50 to 300, while keeping the same monomer proportions. The star polymer charge content was adjusted by varying the molar ratio of the negatively charged PAA block (core) and neutral PMSEA block (shell) in each arm. The star polymer hydrophobicity was adjusted by copolymerizing hydrophilic MSEA with hydrophobic MTEA in different ratios (Figure 1a).

Synthesis of PtBA Core of Star Polymers with DP 25 in Each Arm. The P*t*BA core of star polymer was made by a core first approach. The *β*-CD-21Br ATRP Initiator was first synthesized according to previously published protocol.[31] The P*t*BA star polymer was then synthesized using Supplemental Activation Reducing Agent (SARA) ATRP. Briefly, *β*-CD-21Br initiator (0.1 g, 1.0 equiv), *t*BA (3.16 g, 3.61 mL, 1050 equiv), copper(II) bromide ($CuBr_2$, 0.55 mg, 0.105 equiv), and Me_6TREN (1.7 *μ*L, 0.2625 equiv) and copper wire (diameter 1.0 mm, length 1.0 cm) were added into 3.60 mL of anisole in a sealed Schlenk flask equipped with a stir bar. The reactor was degassed by purging with N_2 for 15 min, and the reaction was allowed to proceed at room temperature. The monomer conversion was monitored with ^{1}H NMR and stopped at ∼50% conversion to yield P*t*BA star polymers with 25 *t*BA repeat units in each arm. The products were purified by dialysis (MWCO = 8000 Da) in methanol for 3 cycles. Molecular weight (*Mn*) and molecular weight distribution (*Đ*) of the P*t*BA star polymers were measured by size exclusion chromatography equipped with a refractive index detector. Star polymers with P*t*BA DP of 75, 125, and 150 were also prepared. Their synthesis procedures are documented in the SI.

Synthesis of $PtBA_{25}$-b-$PMSEA_{125}$ star polymer. The P*t*BA arms were extended with PMSEA blocks by UV light induced photo-ATRP.[32] Briefly, 0.06 g of 25 DP P*t*BA star polymer (1 equiv), 0.713 g of MSEA (5250 equiv), 0.98 mg of $CuBr_2$ (5.25 equiv), and 0.0043 mL of Me_6Tren (18.38 equiv) were dissolved in 4.40 mL of DMF. The reaction was degassed by purging with N_2 for 15 min and proceeded under UV light (36 W) to activate the Me_6Tren ligand and reduce Cu(II) into Cu(I). The monomer conversion was monitored by ^{1}H NMR and stopped at ∼50% conversion to yield a P*t*BA_{25}-*b*-$PMSEA_{125}$ star polymer. The product was purified by dialysis against methanol for three cycles (MWCO = 8000 Da), and the chemical composition of the product was verified by ^{1}H NMR. Synthesis procedures for other PAA-*b*-PMSEA and PAA-*b*-P(MSEA-*co*-MTEA) star polymers used in this study are documented in SI.

Hydrolysis of PtBA-b-PMSEA and PtBA-b-P(MSEA-co-MTEA) Star Polymers. The P*t*BA in P*t*BA-*b*-PMSEA and P*t*BA-*b*-P(MSEA-*co*-MTEA) star polymers were selectively hydrolyzed by TFA[31] to yield the corresponding PAA-*b*-PMSEA and PAA-*b*-P(MSEA-*co*-MTEA) star polymers. A 0.3 g mass of P*t*BA-*b*-PMSEA or P*t*BA-*b*-P(MSEA-*co*-MTEA) star polymer was dissolved in 10 mL of DCM in a 25 mL glass vial with stirring. The polymer solution was placed in an ice bath, and 1 mL of TFA was injected into the solution. The reaction was allowed to warm to room temperature and proceed for ∼24 h. The resulting solution was dialyzed against methanol for three cycles (MWCO = 8000 Da) to remove excess TFA.

Plant Growth. The tomato (*Solanum lycopersicum*) plants used in this study were cultured hydroponically with 1/4 strength Hoagland's solution aerated using air pumps. This comparison of star polymer size, charge, and hydrophobicity is conducted under conditions where plants have easy access to all necessary nutrients. Tomato seeds were rinsed by Milli-Q water twice before they were surface sanitized with 10% bleach for 1 min; they were then thoroughly rinsed with Milli-Q water five times. The sterilized seeds were kept in Milli-Q water in the dark for 24 h before being germinated in a Petri-dish on water-soaked filter paper in the dark for 10 days. The seedlings were then transplanted to 100 mL plastic cups. The plants were grown at lab temperature (∼20 °C) using a 16 h light:8 h dark cycle. Star polymers were foliarly applied to plants after 30 days of growth, in the vegetative stage, with 5 to 6 true leaves, and before flowering.

Gd Loading into Star Polymers for Tracking Their Distribution in Plants. Gd^{3+} was used as a marker to track star polymer uptake and distribution in plants. In a typical procedure, 20 mg of the as synthesized star polymer was dissolved into 5 mL of 0.05 M NaOH water solution in an ice bath with sonication (iSonic P4800). The pH of the polymer solution was then adjusted to 6.5 using aliquots of 0.1 M HCl; 50 mg of $GdCl_3{\cdot}6H_2O$ was then added into the PAA_{25}-*b*-$PMSEA_{25}$, PAA_{25}-*b*-$PMSEA_{125}$, PAA_{75}-*b*-$PMSEA_{75}$ star polymer solutions, and 10 mg of $GdCl_3{\cdot}6H_2O$ was added to PAA_{125}-*b*-$PMSEA_{25}$, PAA_{150}-*b*-$PMSEA_{150}$, PAA_{25}-*b*-P($MSEA_{100}$-*co*-$MTEA_{25}$), and PAA_{25}-*b*-P($MSEA_{75}$-*co*-$MTEA_{50}$) star polymer solutions. Less Gd was added for some polymers to avoid star polymer precipitation, as polymer precipitation causes the solution to become cloudy. The solutions were vortex-mixed for 24 h to allow partitioning of Gd^{3+} into the PAA core of the star polymers before being dialyzed against 200 mL Milli-Q water for seven cycles, until free Gd concentration in the dialysate contained less than 0.1% of Gd loaded in star polymers (MWCO = 8000 Da). The Gd loaded star polymer samples (0.05 mL) were digested by 0.5 mL of 70% HNO_3 at room temperature for 30 min, then diluted to 5 mL with Milli-Q water before analyzed by ICP-MS (Agilent 7700X). Gd loading results are shown in Table S1. The stability of Gd loaded star polymer in plant leaves was evaluated in simulated leaf apoplastic fluid at pH 5.5 (Table S2).[33] The Gd leaching result is shown in Table S3. Less than

https://doi.org/10.1021/acs.est.1c01065
Environ. Sci. Technol. 2021, 55, 10758−10768

0.5% of loaded Gd leached out of Gd loaded star polymers in simulated plant apoplastic fluid after 24 h.

Star Polymer Foliar Exposure, Uptake, and Transport in Tomato Plants. The Gd-loaded star polymers were applied to tomato leaves in aqueous 0.1 vol % Silwet L-77 spreading agent solution to promote spreading on the leaf surface. Silwet is a nonionic agricultural surfactant commonly used as a wetting agent for agrochemical sprays.[11] Each treatment included 5−6 replicate plants. All of the star polymers were well dispersed before foliar application (Table S4). We deposited 20 μL of a 1 g L^{-1} star polymer solution as 4 drops with 5 μL in each (20 μg of star polymer total). Each drop was applied to a different location on the adaxial side of the second true leaf to fully cover the leaf. One gram per liter star polymer concentration was used, as this concentration of a similar polymer did not cause a significant toxicity effect to plants in our previous study.[2] The plants were harvested 3 days after exposure, consistent with our previous study.[2] Each plant was cut into five parts: leaf where the Gd-loaded star solutions were applied (denoted as "exposed zone"), leaves at growth stages lower than the exposed leaves (denoted as "younger leaf"), leaves at growth stages higher than exposed leaves (denoted as "older leaf"), stem of the plant (denoted as "stem"), and roots (denoted as "root").

To determine star polymer transport to different plant compartments, the Gd^{3+} content in different plant tissues were measured. All plant samples were first dried at 105 °C for 24 h to remove water. The dried plant tissues were weighed and digested overnight at room temperature with 1 mL of a 2:1 mixture of 70% HNO_3 and 30% H_2O_2, followed by heating at 100 °C for 45 min.[2,34] Post digestion, the samples were diluted to 5% HNO_3 by Milli-Q water and filtered through a 0.45 μm PTFE syringe filter before analysis by ICP-MS.

Crystal Violet Loading and Star Polymer Foliar Application to Image NP-Leaf Interactions. To assess star polymer-leaf interactions, the star polymers were loaded with crystal violet (CV) before foliar exposure and imaging. Briefly, 10 mg of PAA_{25}-*b*-$PMSEA_{125}$ or PAA_{25}-*b*-P($MSEA_{75}$-*co*-$MTEA_{50}$) star polymers was dissolved into 5 mL of 0.05 M NaOH water solution in an ice bath with sonication. The pH of the polymer solution was then adjusted to 6.5 by 0.1 M NaOH and HCl. A 1 mg portion of CV was then added into the star polymer solutions, and the mixture was vortex mixed for 24 h. The solution was dialyzed against 1 L of Milli-Q water (MWCO = 8000) to remove free CV. The integrity of CV loading within similar star polymers based on PAA binding at 20 °C was confirmed experimentally in our previous work.[2]

The CV-loaded star polymer solutions were mixed with or without 0.1 vol % Silwet L-77 surfactant before foliar application. Four drops of 5 μL of CV-loaded star polymer solution at 1 g L^{-1} polymer concentration was applied. The exposed leaves were incubated for 2 days before imaging to assess the star polymer leaf uptake pathway with or without Silwet L-77. While different from the star polymer translocation assessment, 2 days is sufficient to observe the differences.

Imaging Polymer-Leaf Interactions. The distribution of CV-loaded star polymers in tomato leaves was assessed using an enhanced dark-field microscope coupled to a hyperspectral imaging system (CytoViva Inc.) as previously described.[2] Briefly, this enhanced resolution dark-field microscope system (BX51, Olympus,) was equipped with a 150 W halogen light source and a hyperspectral camera (CytoViva hyperspectral imaging system 1.4). The leaves were imaged in air at 10× or in oil immersion at 60× magnification. Hyperspectral images were acquired using 75% light source intensity and 0.1 to 0.5 s acquisition per line and corrected for the lamp contribution. The focal planes for hyperspectral images included the leaf surface (above the cuticle) and the epidermis cell layer. The spectral library for hyperspectral mapping was built using images of CV-loaded star polymers in plant leaves as described in SI. The spectral library was used to identify pixels with CV-loaded star polymers in order to map their locations in exposed leaves using spectral angle mapping (SAM, ENVI 5.2).

RESULTS AND DISCUSSION

Synthesis and Characterization of Star Polymers with Different Size, Charge Content, and Hydrophobicity. The theoretical molecular weight and chemical compositions of PAA-*b*-PMSEA and PAA-*b*-P(MSEA-*co*-MTEA) star polymers were calculated according to the molar ratios between P*t*BA, PMSEA, and PMTEA in each star polymer, measured by ^{1}H NMR (Figure S1). The calculated number-average molecular weights (M_n) of the different star polymers are shown in Table S4. The low dispersity of the star polymers was confirmed by GPC. P*t*BA star polymers having arms with DP = 25, 75, 125, and 150 DP had dispersity $Đ$ = 1.05, 1.02, 1.04 and 1.11, respectively (Figure S2).

The size, charge content, and hydrophobicity of the star polymers were adjusted by varying the length and chemical composition of polymer arms (Figure 1a,c). As shown in Figure 1a and Figure S1, the PAA_{25}-*b*-$PMSEA_{25}$, PAA_{75}-*b*-$PMSEA_{75}$, and PAA_{150}-*b*-$PMSEA_{150}$ star polymers, with the same 1:1 PAA to PMSEA molar ratio, have hydrodynamic diameters ranging from 6 nm for the smallest polymer to 35 nm for the largest polymer (Figure 1b, Figure S3). The electrophoretic mobility was measured in similar solutions using a Malvern zetasizer. Apparent zeta potentials (ζ), recognizing that such potentials are only apparent when applying the rigid particle Smoluchowski model to soft colloids, ranged from −22.6 ± 2.3 to −30.4 ± 2.7 mV (Figure 1a). The electrophoretic mobility was measured with Gd-loaded star polymers to represent the properties of the polymers tracked in leaves.

The PAA_{25}-*b*-$PMSEA_{125}$, PAA_{75}-*b*-$PMSEA_{75}$, and PAA_{125}-*b*-$PMSEA_{25}$ star polymers have different relative amounts of PAA and PMSEA, ranging from 17% PAA for the least charged polymer to 83% PAA repeating units in each arm for the most highly charged sample (Figure 1a, Figure S1c,f,g). With arms of different PAA:PMSEA ratios but a constant total DP, these star polymers have similar hydrodynamic diameters of ∼20 nm and increasingly negative zeta potentials with increasing PAA content (Figure 1a,b, Figure S3). The Gd-loaded PAA_{125}-*b*-$PMSEA_{25}$ star polymer had the most negative ζ of −31.7 ± 0.6 mV (EPM of −2.48 ± 0.05 μm cm V^{-1} s^{-1}), while the PAA_{25}-*b*-$PMSEA_{125}$ star polymer had the least negative ζ of −11.9 ± 0.8 mV (EPM of −0.94 ± 0.06 μm cm V^{-1} s^{-1}) (Figure 1a, Table S4).

The hydrophilic MSEA was copolymerized with 20−40% hydrophobic MTEA to synthesize star polymers with different hydrophobicity (Figure 1a,c). Polymer hydrophobicity was assessed by measuring the optical density at 541 nm (Agilent Cary 5000) of solutions in 1 cm square cuvettes (0.5 g L^{-1}) as a function of pH at 20 °C. At pH < 4, PAA protonation decreases the charge and electrostatic repulsion between star polymers,[35,36] allowing the hydrophobic MTEA block to drive

https://doi.org/10.1021/acs.est.1c01065
Environ. Sci. Technol. 2021, 55, 10758−10768

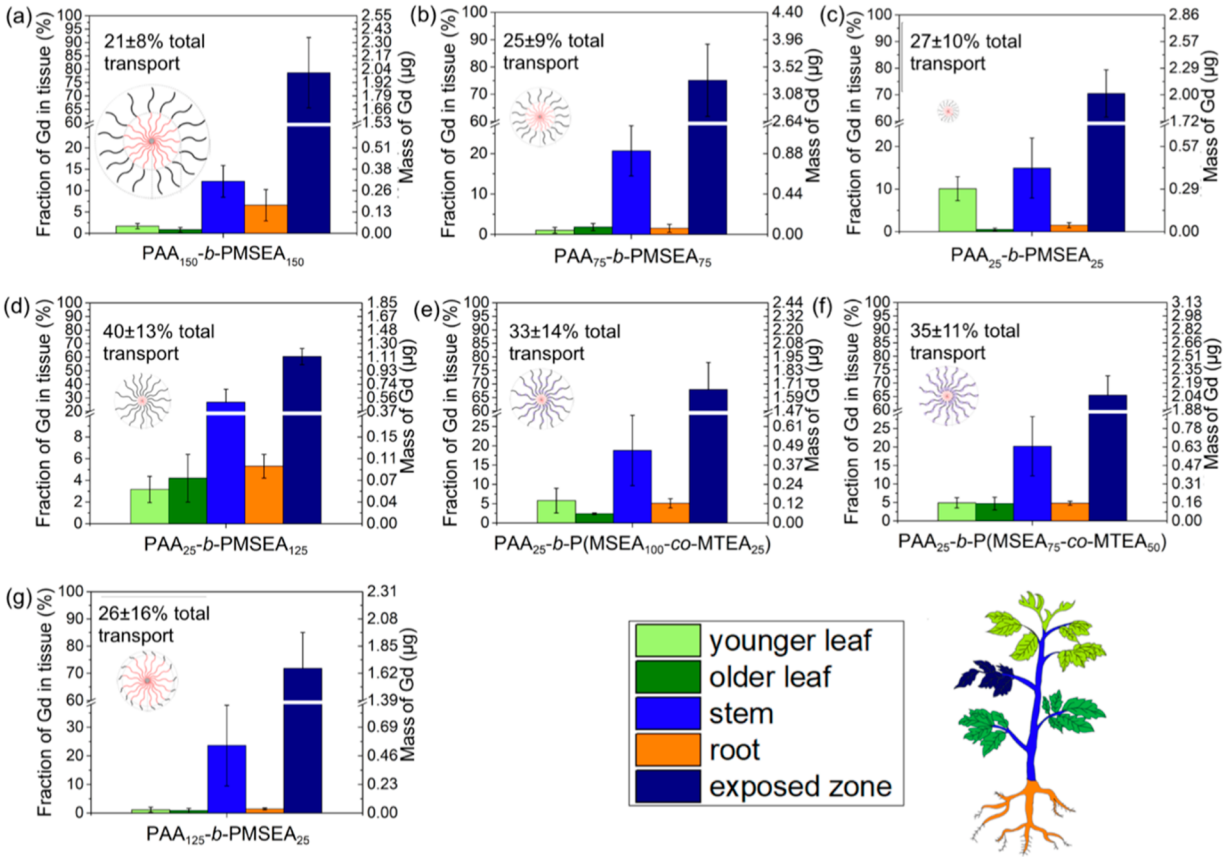

Figure 2. Uptake and transport of foliarly applied Gd loaded star polymers in tomato plants with 0.1 v/v% Silwet L-77 surfactant for (a) PAA_{150}-*b*-$PMSEA_{150}$ star polymers, (b) PAA_{75}-*b*-$PMSEA_{75}$ star polymers, (c) PAA_{25}-*b*-$PMSEA_{25}$ star polymers, (d) PAA_{25}-*b*-$PMSEA_{125}$ star polymers, (e) PAA_{25}-*b*-P($MSEA_{100}$-*co*-$MTEA_{25}$) star polymers, (f) PAA_{25}-*b*-P($MSEA_{75}$-*co*-$MTEA_{50}$) star polymers, and (g) PAA_{125}-*b*-$PMSEA_{25}$ star polymers at 1.0 g L^{-1} exposure, expressed by both percentage and weight of Gd detected in each plant compartment. Five to six plants were used for each treatment. Error bars represent standard deviations.

aggregation. As shown in Figure 1d, the most hydrophobic PAA_{25}-*b*-P($MSEA_{75}$-*co*-$MTEA_{50}$) star polymers aggregated at pH ∼ 4, while the relatively less hydrophobic PAA_{25}-*b*-P($MSEA_{100}$-*co*-$MTEA_{25}$) star polymer did not aggregate until pH < 3.0, and the hydrophilic PAA_{25}-*b*-$PMSEA_{125}$ star polymer did not aggregate even at pH < 2.0. Star polymers with less MTEA require lower pH and more charge neutralization to allow aggregation. The dispersibility of the more hydrophobic star polymers in water is a result of the electrostatic charge residing in the PAA blocks of each star polymer.

Star Polymer Uptake and Phloem Loading. Tomato plants (*Solanum lycopersicum*) were used as model system to evaluate star polymer uptake, phloem loading, and transport after foliar application. The star polymers that have moved from the exposed leaf to other plant organs are assumed to have been loaded into the phloem translocated to stem, roots, and young leaves, as the phloem is the vascular tissue responsible for long distance transport of photosynthetic products from mature leaves to these organs.[19] Figure 2 shows the Gd mass and percent of total applied Gd found in different plant organs. To better visualize how the star polymer properties affected transport, Figure 3 shows the percent of the phloem loaded star polymers that have transported to different plant organs.

In our previous study, 1.4−2% of the star polymer was observed to transport out of exposed leaf without Silwet L-77.[2] When star polymers are applied with a commonly used surfactant Silwet L-77, all of the star polymers showed similar ∼30 ± 7% phloem transport 3 days after exposure, regardless of size, negative charge content, and hydrophobicity (Figure 2a−g, Figure S4). The leaf phloem loading process is not significantly affected by these properties for these star polymers. Also, the size cutoff for star polymer phloem loading and translocation is evidently larger than 35 nm in tomato plants (a dicot). This is larger than the previously reported size exclusion limits (∼20 nm) estimated for engineered metal and metal oxide NP transport in pea (*Pisum sativum*) plants.[37,38] About 15 to 24% of the applied star polymer mass ended up in the stem of the plant, with no specific trend in the accumulated mass observed for the different star polymer properties (Figure 2a−g). Because not all of the applied polymer was phloem loaded, this corresponds to a majority (∼55−83%) of the phloem loaded star polymers that end up in the stem (Figure 3). This is consistent with a previous study of foliar application a PAA-*b*-PNIPAm star polymer on tomato plants.[2] However, some fraction of the star polymers was also found in older leaves for all of the polymer architectures used here (Figure 3), suggesting some xylem transport. Mature leaves stop importing phloem materials from the rest of the plant and begin to export photosynthesis products through phloem.[39] Therefore, in older leaves as fully mature leaves, phloem sap flow goes outward and the star polymers could transport to older leaves only through xylem flow. The exchange of sap that occurs between the phloem and xylem is the most likely explanation for this

https://doi.org/10.1021/acs.est.1c01065
Environ. Sci. Technol. 2021, 55, 10758−10768

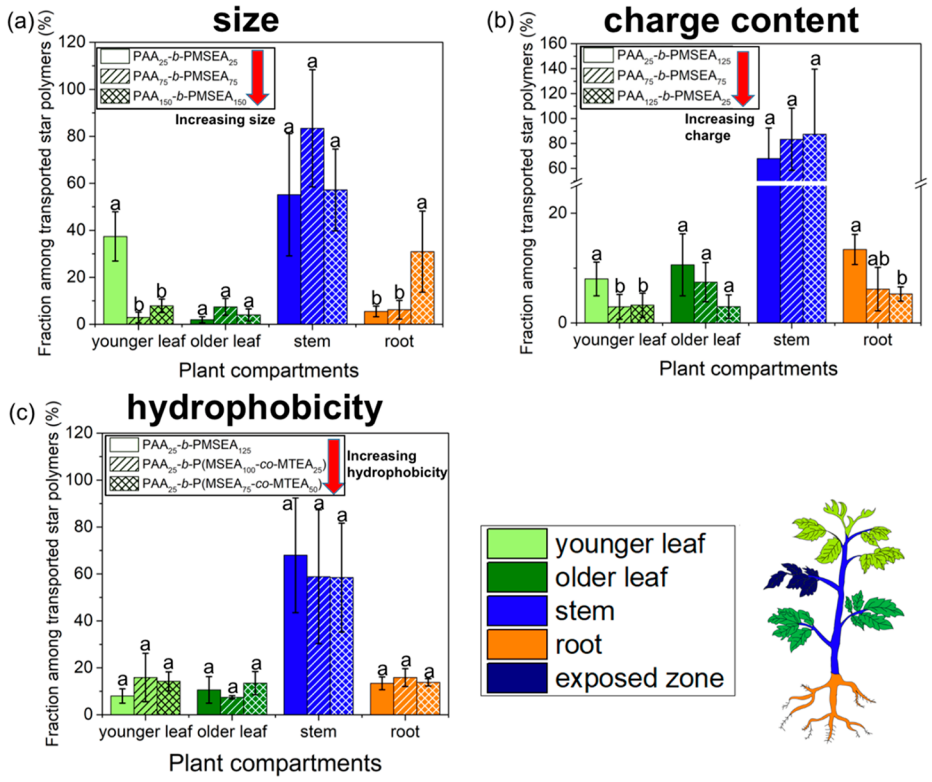

Figure 3. Fraction of transported (phloem loaded) star polymers from exposed leaves to different organs of tomato plants. (a) PAA_{25}-*b*-$PMSEA_{25}$, PAA_{75}-*b*-$PMSEA_{75}$, and PAA_{150}-*b*-$PMSEA_{150}$ star polymers with different hydrodynamic sizes. (b) PAA_{125}-*b*-$PMSEA_{25}$, PAA_{75}-*b*-$PMSEA_{75}$, and PAA_{25}-*b*-$PMSEA_{125}$ star polymers with different charge content and (c) PAA_{25}-*b*-$PMSEA_{125}$, PAA_{25}-*b*-P($MSEA_{100}$-*co*-$MTEA_{25}$), and PAA_{25}-*b*-P($MSEA_{75}$-*co*-$MTEA_{50}$) star polymers with different hydrophobicity. Error bars represent standard deviations for 5−6 replicates. ANOVA test followed by Fisher's LSD test for multiple comparisons, $P \leq 0.05$.

observation.[40] The star polymer treatments did not show significant differences in their transport to older leaves indicating that the polymer design parameters did not significantly affect phloem-xylem nanoparticle exchange.

Effect of Size on Star Polymer Transport in Plants. The PAA_{25}-*b*-$PMSEA_{25}$, PAA_{75}-*b*-$PMSEA_{75}$, and PAA_{150}-*b*-$PMSEA_{150}$ star polymers with similar charge content (50% negatively charged PAA, Figure S1g−i) but different sizes ranging from 6 to 35 nm have different distributions in the plant compartments. According to Figure 2a−c, the small (6 nm) PAA_{25}-*b*-$PMSEA_{25}$ star polymers (Figure 2c) moved more readily to the younger leaves of tomato plants, with approximately 10% of the applied mass ending up in the younger leaves. This corresponds to 37.4% of the phloem loaded star polymers and is over four times higher than the transport of larger 20−35 nm star polymers to younger leaves ($P \leq 0.05$) (Figure 3a). Phloem unloading is needed for star polymers to access nonvascular compartments and requires a symplastic transport step in leaves.[39,41] Previous studies have suggested that smaller NPs may favor symplastic transport because the size cutoffs for NP transport through cell walls and plasmodesmata are considered to be ∼20 nm.[18,42] This size exclusion effect on NPs moving between vascular and nonvascular tissue may be inhibiting more of the larger star polymers from getting into younger leaves.[37,43] However, a finite fraction of the larger star polymers did make it to the younger leaves, so the 20 nm size cutoff is not strict.

The largest PAA_{150}-*b*-$PMSEA_{150}$ star polymer (35 nm) was mostly distributed to the stem and roots (Figure 2a). With 30.9% of the phloem-loaded PAA_{150}-*b*-$PMSEA_{150}$ star polymers found in roots (Figure 3a), this was more than five times higher root accumulation compared to the sub-20 nm star polymers ($P \leq 0.05$). The default pathway of root phloem unloading is through apoplasts, especially in the root cell expansion zone.[25] Apoplastic transport in plants should be favored for larger NPs, while the smaller NPs more likely transport through symplastic pathways.[42,44] Therefore, the higher accumulation of larger star polymers in roots could be explained by higher phloem unloading of large star polymers through an apoplastic pathway. Similarly, 3 nm AuNPs were found to transport preferentially to young shoots of plants, while the larger sized (50 nm) AuNPs tended to accumulate in plant roots after foliar application.[3] This suggests that star polymers and rigid metal NPs may behave similarly in this regard.

Effect of Charge Content on Star Polymer Transport in Plants. Negative charge content also significantly affected the distribution of star polymers after foliar exposure. The Gd-loaded PAA_{25}-*b*-$PMSEA_{125}$ star polymers, with a smaller magnitude apparent ζ potential (−11.9 ± 0.8 mV and EPM −0.94 ± 0.06 μm cm V^{-1} s^{-1}) compared to PAA_{75}-*b*-$PMSEA_{75}$ (ζ potential = −26.8 ± 0.5 mV, EPM = −2.09 ± 0.04 μm cm V^{-1} s^{-1}) and PAA_{125}-*b*-$PMSEA_{25}$ (ζ potential = −31.7 ± 0.5 mV, EPM = −2.48 ± 0.05 μm cm V^{-1} s^{-1}), had greater transport into nonvascular tissues (Figure 2b,d,g and Figure 3b). The fraction of phloem-loaded PAA_{25}-*b*-$PMSEA_{125}$ star polymers transported into younger leaves and roots is twice that of the higher charge content PAA_{75}-*b*-$PMSEA_{75}$ and PAA_{125}-*b*-$PMSEA_{25}$ star polymers (Figure 3b). Thus, the lower

https://doi.org/10.1021/acs.est.1c01065
Environ. Sci. Technol. 2021, 55, 10758−10768

charge content star polymers facilitate long distance transport through the vasculature to other plant organs.

The reasons for the influence of charge on translocation are likely a result of tissue-star polymer interactions. The star polymers with higher charge content and thinner neutral PMSEA passivation shell present a more negative electrical potential to plant mesophyll and phloem conducting cells. The PAA_{75}-*b*-$PMSEA_{75}$ and PAA_{125}-*b*-$PMSEA_{25}$ star polymers have a net negative apparent ζ potential exceeding −25 mV (EPM exceeding −2 μm cm V^{-1} s^{-1}) (Figure 1a). High NP charge has been demonstrated to promote plant protoplast and chloroplast uptake that results in the NPs becoming kinetically trapped within plant cell or organelle lipid bilayers.[26,45] The star polymers having high content charge may have a lower mobility in plant cells and organelles due to their interactions with lipid membranes that reduces their long distance transport in plants.

We hypothesize that this significant negative electrical potential could also be triggering the plant immune system. The plant immune system detects multivalent ions and stops their spread by expressing a glycine-rich protein cdiGRP, elevating the Callose (1,3-β-D-glucan) level in the vasculature to reinforce the cell wall and create a boundary between the vascular and nonvascular tissue.[21,46] This immune mechanism has been reported to inhibit systemic transport of tobacco mosaic virus (TMV) in plants.[20] Star polymers with a similar smallest dimension and charge to TMV (diameter ∼10 nm, apparent ζ potential ∼ −35 mV at pH 7.5) may also be trapped through this plant defense mechanism.[47] Our data suggests that the immune regulation may be more restrictive to the higher charge content star polymers compared with the lower charge content ones. Apart from the plant immune response, the plant cell wall can also stop extraneous agents from moving in plants.[48] For instance, multivalent metal ions can be immobilized in the stem by binding with cellulose on the cell wall.[48] A possible role of direct star polymer interactions with cell wall components cannot be ruled out.

Star Polymer Hydrophobicity Affect Their Foliar Uptake Pathway. Transport results for PAA_{25}-*b*-$PMSEA_{125}$, PAA_{25}-*b*-P($MSEA_{100}$-*co*-$MTEA_{25}$), and PAA_{25}-*b*-P($MSEA_{75}$-*co*-$MTEA_{50}$) star polymers that have similar charge content and hydrodynamic diameters but different hydrophobicities are shown in Figure 2d,e,f. Star polymers with higher MTEA content are more hydrophobic (Figure 1b,c). Total translocation (phloem loading) and star polymer distributions in different plant organs are similar for the different hydrophobicities (Figure 3c). The absence of an effect of hydrophobicity in transport was not expected. This is because Silwet L-77 (0.1 wt %) lowers the surface tension of the applied polymer solution to promote wetting and uptake through stomatal pores, and it also disturbs the cuticle and epidermis cells.[2,11] The latter helps the star polymers to penetrate through the cuticle and epidermis and enter the mesophyll, and ultimately load into the phloem, regardless of their hydrophobicity.[2,11]

We confirmed this by measuring the distribution of CV-loaded star polymers in tomato leaves using DF-HSI. The effectiveness of spectral library to pick up CV loaded star polymers signals is confirmed by mapping the control images (Figure S6). As shown in Figure S7, the CV-loaded star polymers could not be detected on the leaf surface (above the cuticle) or in or above the epidermis layer when CV loaded star polymers were applied together with Silwet L-77 for both PAA-*b*-PMSEA and PAA-*b*-P(MSEA-*co*-MTEA) star polymers. This indicates that nearly all of the applied star polymers penetrated more deeply and accessed the mesophyll.[2,11,49]

When applied without surfactants, the star polymers with different hydrophobicity do interact with tomato leaves differently. As shown in Figure 4a−f, both the hydrophilic PAA_{25}-*b*-$PMSEA_{125}$ and hydrophobic PAA_{25}-*b*-P($MSEA_{75}$-*co*-$MTEA_{50}$) star polymers are present on the leaf surface (Figure 4c,f). However, the more hydrophilic PAA_{25}-*b*-$PMSEA_{125}$ star polymer is taken up into the epidermis layer through cuticle penetration, as more CV-loaded star polymers were found in the epidermis cell layer (Figure 4a,b). In contrast, the more hydrophobic PAA_{25}-*b*-P($MSEA_{75}$-*co*-$MTEA_{50}$) star polymers were found to accumulate mainly at the bases of trichomes in the epidermis layer (Figure 4e). The presence of the relatively more hydrophobic PAA_{25}-*b*-P($MSEA_{75}$-*co*-$MTEA_{50}$) star polymers in the epidermis was much less than their more hydrophilic counterparts (Figure 4b,e). This is possibly due to stronger interaction between the more hydrophobic star polymer and the similarly lipophilic tomato leaf cuticle,[50] which potentially inhibits hydrophobic star polymers from penetrating through and being taken up into the epidermis layer. A previous study also showed that Au NPs with a more hydrophobic surface coating adhere more strongly to wheat cuticle, which potentially inhibits their further transport.[3] Recent studies have also shown that trichomes can be an important pathway for NP adsorption and accumulation.[3,51,52] This study also indicates that trichomes may be a significant uptake pathway for relatively hydrophobic star polymers in the absence of a surfactant spreading agent. These results suggest that foliar applied polymer nanocarriers may be designed to target specific locations, e.g., epidermis or trichomes, by selecting appropriate properties.

Environmental Implications. In this study, we synthesized star polymers with different size, negative charge content, and hydrophobicity and tested their uptake, phloem loading and biodistribution after foliar application. The star polymers have significantly more efficient uptake and phloem loading (30%) than those of conventional active ingredients (0.1%) and micronutrients (5%). When loaded with active agents or micronutrients, enhanced uptake and transport efficiency achieved by star polymers could potentially help reduce agrochemical application rates and losses, which would alleviate the environmental burden caused by agrochemical runoff into natural water and soil.

Apart from high phloem loading, the star polymers with lower negative charge content exhibit higher translocation to nonvascular tissues such as younger leaves and older leaves and to roots. Smaller star polymers better translocate to younger leaves, and larger star polymers have higher accumulation in roots. Therefore, star polymers with different sizes and charges can be used for targeted agent delivery into different plant compartments. These findings can help in the rational design of polymer based nanocarriers, enabling targeted and more effective plant disease control. This study also suggests that star polymers with different hydrophobicity could interact with plant leaves differently when applied without surfactants, with the more hydrophilic star polymers showing better penetration through cuticle toward the epidermis cell layer, while the more hydrophobic counterpart transports to the epidermis layer mainly through trichomes on the leaf surface. This indicates hydrophobicity of nanocarriers can affect their uptake into leaf epidermis for agents applied without surfactants.

https://doi.org/10.1021/acs.est.1c01065
Environ. Sci. Technol. 2021, 55, 10758−10768

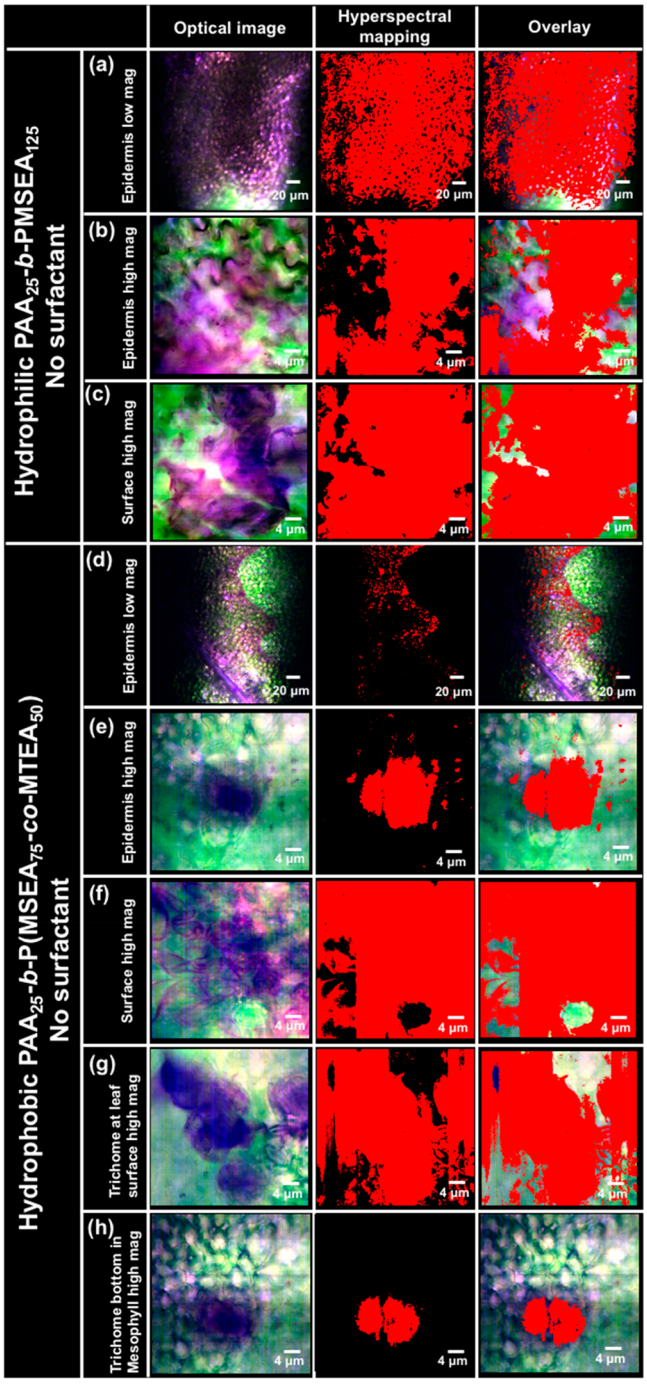

Figure 4. Interactions of CV loaded PAA_{25}-*b*-$PMSEA_{125}$ and PAA_{25}-*b*-P($MSEA_{75}$-*co*-$MTEA_{50}$) star polymers with tomato leaves applied *without surfactants* assessed by enhanced dark field hyperspectral imaging. Images show the leaf surface, the epidermis and both low and high magnification, and leaf trichomes. Pixels containing the CV loaded polymers are highlighted in red based on their hyperspectral signature (Figure S5). Hyperspectral detection of CV-loaded star polymers is described in detail in the SI along with a hyperspectral library used for identifying CV loaded star polymers.

Apart from rationalizing the design of nanocarriers that can potentially deliver agrochemicals, studying the fate and transport behaviors of these softer polymer NPs is also critical to assess their potential risk of exposure. In spite of the differences in rigidity between the star polymers used here and the more studied metal and metal oxide NPs, the effect of the size of the star polymers on transport in the plants was similar as was reported for AuNPs after foliar application,[3] suggesting that the softer nature of star polymers may not play a significant role in their interactions with plant organs. Future research needs to focus on understanding the phloem loading pathway and mechanism after star polymers enter the mesophyll. This could potentially increase phloem loading to higher than the 30% observed here. Protein corona formation as a function of nanocarrier property could also drive the in-planta distribution differences and should be further studied.[53] Also, the long-term fate of star polymers in plants is still unknown. The transport of star polymers to fruit or other edible parts of the crop plants needs to be measured to evaluate the risk of exposure to human consumption. Plant health related parameters, including photosynthesis and growth after star polymer application, will also provide a better understanding of the effect of polymer nanocarriers on plant health. Finally, the capacity of star polymers for loading and delivering real agrochemicals must be examined to confirm their potential to manage plant disease and supply nutrients. Different cargo molecules loaded into star polymers can also neutralize their charge differently and affect their transport behaviors. Therefore, the uptake and transport of star polymers also have to be examined with different loaded materials in future studies.

■ ASSOCIATED CONTENT

Supporting Information

The Supporting Information is available free of charge at https://pubs.acs.org/doi/10.1021/acs.est.1c01065.

Synthesis protocols of P*t*BA-*b*-PMSEA and P*t*BA-*b*-P(MSEA-*co*-MTEA) star polymers, procedures for spectral library build up in hyperspectral imaging, ^{1}H NMR spectra of MSEA, MTEA monomers and all of P*t*BA-*b*-PMSEA and P*t*BA-*b*-P(MSEA-*co*-MTEA) star polymers before hydrolysis, the GPC trace of P*t*BA star polymers with different DP P*t*BA arms, spectral library used for mapping CV loaded star polymers, the control hyperspectral images without CV loaded star polymers, interaction between star polymer and tomato plants with 0.1 vol % Silwet L-77, Gd^{3+} loading in PAA-*b*-PMSEA and PAA-*b*-P(MSEA-*co*-MTEA) star polymers measured by ICP-MS, composition of simulated plant apoplastic fluid, Gd leaching out of star polymer after dialysis in simulated apoplastic fluid and EPM and apparent zeta potential of star polymers with/without Gd loading (PDF)

■ AUTHOR INFORMATION

Corresponding Authors

Gregory V. Lowry − *Department of Civil and Environmental Engineering and Center for Environmental Implications of Nano Technology (CEINT), Carnegie Mellon University, Pittsburgh, Pennsylvania 15213, United States;* orcid.org/0000-0001-8599-008X; Phone: (412) 268-2948; Email: glowry@cmu.edu; Fax: (412) 268-7813

Robert D. Tilton − *Center for Environmental Implications of Nano Technology (CEINT), Department of Chemical Engineering, and Department of Biomedical Engineering, Carnegie Mellon University, Pittsburgh, Pennsylvania 15213, United States;* orcid.org/0000-0002-6535-9415;

https://doi.org/10.1021/acs.est.1c01065
Environ. Sci. Technol. 2021, 55, 10758−10768

Phone: (412) 268-2948; Email: tilton@cmu.edu; Fax: (412) 268-7813

Authors

Yilin Zhang − *Department of Civil and Environmental Engineering and Center for Environmental Implications of Nano Technology (CEINT), Carnegie Mellon University, Pittsburgh, Pennsylvania 15213, United States;* orcid.org/0000-0003-4246-3620

Liye Fu − *Department of Chemistry, Carnegie Mellon University, Pittsburgh, Pennsylvania 15213, United States;* orcid.org/0000-0002-7077-5632

Sipei Li − *Department of Chemistry, Carnegie Mellon University, Pittsburgh, Pennsylvania 15213, United States;* orcid.org/0000-0001-7659-1001

Jiajun Yan − *Department of Chemistry, Carnegie Mellon University, Pittsburgh, Pennsylvania 15213, United States;* orcid.org/0000-0003-3286-3268

Mingkang Sun − *Department of Chemistry, Carnegie Mellon University, Pittsburgh, Pennsylvania 15213, United States;* orcid.org/0000-0003-4652-5243

Juan Pablo Giraldo − *Department of Botany and Plant Sciences, University of California, Riverside, California 92521, United States;* orcid.org/0000-0002-8400-8944

Krzysztof Matyjaszewski − *Department of Chemistry, Carnegie Mellon University, Pittsburgh, Pennsylvania 15213, United States;* orcid.org/0000-0003-1960-3402

Complete contact information is available at: https://pubs.acs.org/10.1021/acs.est.1c01065

Notes

The authors declare no competing financial interest.

■ ACKNOWLEDGMENTS

This research is partially supported by the National Science Foundation (NSF) and the US Environmental Protection Agency (EPA) under NSF Cooperative Agreement EF-1266252, Center for the Environmental Implications of Nanotechnology (CEINT). G.V.L., J.P.G., and Y.Z. acknowledge support from NSF CBET-1911763. K.M., L.F., S.L., J.Y., and M.S. acknowledge support by NSF DMR 1501324. Any opinions, findings, conclusions or recommendations expressed in this material are those of the author(s) and do not necessarily reflect the views of the NSF or the EPA. This work has not been subjected to EPA review and no official endorsement should be inferred.

■ REFERENCES

(1) Luo, J.; Huang, X.; Jing, T.; Zhang, D.; Li, B.; Liu, F. Analysis of Particle Size Regulating the Insecticidal Efficacy of Phoxim Polyurethane Microcapsules on Leaves. *ACS Sustainable Chem. Eng.* **2018**, *6*, 17194.

(2) Zhang, Y.; Yan, J.; Avellan, A.; Gao, X.; Matyjaszewski, K.; Tilton, R. D.; Lowry, G. V. Temperature- And PH-Responsive Star Polymers as Nanocarriers with Potential for in Vivo Agrochemical Delivery. *ACS Nano* **2020**, *14* (9), 10954−10965.

(3) Avellan, A.; Yun, J.; Zhang, Y.; Spielman-Sun, E.; Unrine, J. M.; Thieme, J.; Li, J.; Lombi, E.; Bland, G.; Lowry, G. V. Nanoparticle Size and Coating Chemistry Control Foliar Uptake Pathways, Translocation, and Leaf-to-Rhizosphere Transport in Wheat Article. *ACS Nano* **2019**, *13*, 5291−5305.

(4) Spielman-Sun, E.; Lombi, E.; Donner, E.; Howard, D.; Unrine, J. M.; Lowry, G. V. Impact of Surface Charge on Cerium Oxide Nanoparticle Uptake and Translocation by Wheat (*Triticum Aestivum*). *Environ. Sci. Technol.* **2017**, *51* (13), 7361−7368.

(5) Wimalawansa, S. A.; Wimalawansa, J. *Agrochemical-Related Environmental Pollution: Effects on Human Health*; Vol. 3.

(6) Cai, D.; Wu, Z.; Jiang, J.; Wu, Y.; Feng, H.; Brown, I. G.; Chu, P. K.; Yu, Z. Controlling Nitrogen Migration through Micro-Nano Networks. *Sci. Rep.* **2015**, *4*, 1−8.

(7) Wu, H.; Tito, N.; Giraldo, J. P. Anionic Cerium Oxide Nanoparticles Protect Plant Photosynthesis from Abiotic Stress by Scavenging Reactive Oxygen Species. *ACS Nano* **2017**, *11* (11), 11283−11297.

(8) Giraldo, J. P.; Landry, M. P.; Faltermeier, S. M.; McNicholas, T. P.; Iverson, N. M.; Boghossian, A. A.; Reuel, N. F.; Hilmer, A. J.; Sen, F.; Brew, J. A. Plant Nanobionics Approach to Augment Photosynthesis and Biochemical Sensing. *Nat. Mater.* **2014**, *13* (4), 400−408.

(9) Zhu, J.; Li, J.; Shen, Y.; Liu, S.; Zeng, N.; Zhan, X.; White, J. C.; Gardea-Torresdey, J.; Xing, B. Mechanism of Zinc Oxide Nanoparticle Entry into Wheat Seedling Leaves. *Environ. Sci.: Nano* **2020**, *7* (12), 3901.

(10) Zhang, H.; Lu, L.; Zhao, X.; Zhao, S.; Gu, X.; Du, W.; Wei, H.; Ji, R.; Zhao, L. Metabolomics Reveals the "Invisible" Responses of Spinach Plants Exposed to CeO2 Nanoparticles. *Environ. Sci. Technol.* **2019**, *53* (10), 6007−6017.

(11) Hu, P.; An, J.; Faulkner, M. M.; Wu, H.; Li, Z.; Tian, X.; Giraldo, J. P. Nanoparticle Charge and Size Control Foliar Delivery Efficiency to Plant Cells and Organelles. *ACS Nano* **2020**, *14*, 7970−7986.

(12) Xiong, T.; Dumat, C.; Dappe, V.; Vezin, H.; Schreck, E.; Shahid, M.; Pierart, A.; Sobanska, S. Copper Oxide Nanoparticle Foliar Uptake, Phytotoxicity, and Consequences for Sustainable Urban Agriculture. *Environ. Sci. Technol.* **2017**, *51* (9), 5242−5251.

(13) Hong, J.; Peralta-Videa, J. R.; Rico, C.; Sahi, S.; Viveros, M. N.; Bartonjo, J.; Zhao, L.; Gardea-Torresdey, J. L. Evidence of Translocation and Physiological Impacts of Foliar Applied CeO2 Nanoparticles on Cucumber (Cucumis Sativus) Plants. *Environ. Sci. Technol.* **2014**, *48* (8), 4376−4385.

(14) Wang, W. N.; Tarafdar, J. C.; Biswas, P. Nanoparticle Synthesis and Delivery by an Aerosol Route for Watermelon Plant Foliar Uptake. *J. Nanopart. Res.* **2013**, DOI: 10.1007/s11051-013-1417-8.

(15) Karny, A.; Zinger, A.; Kajal, A.; Shainsky-Roitman, J.; Schroeder, A. Therapeutic Nanoparticles Penetrate Leaves and Deliver Nutrients to Agricultural Crops. *Sci. Rep.* **2018**, *8* (1), 1−10.

(16) Santana, I.; Wu, H.; Hu, P.; Giraldo, J. P. Targeted Delivery of Nanomaterials with Chemical Cargoes in Plants Enabled by a Biorecognition Motif. *Nat. Commun.* **2020**, *11* (1), 1−12.

(17) Demirer, G. S.; Zhang, H.; Matos, J. L.; Goh, N. S.; Cunningham, F. J.; Sung, Y.; Chang, R.; Aditham, A. J.; Chio, L.; Cho, M.-J. High Aspect Ratio Nanomaterials Enable Delivery of Functional Genetic Material without DNA Integration in Mature Plants. *Nat. Nanotechnol.* **2019**, *14*, 456.

(18) Zhai, G.; Walters, K. S.; Peate, D. W.; Alvarez, P. J. J.; Schnoor, J. L. Transport of Gold Nanoparticles through Plasmodesmata and Precipitation of Gold Ions in Woody Poplar. *Environ. Sci. Technol. Lett.* **2014**, *1* (2), 146−151.

(19) Jensen, K. H.; Berg-Sørensen, K.; Bruus, H.; Holbrook, N. M.; Liesche, J.; Schulz, A.; Zwieniecki, M. A.; Bohr, T. Sap Flow and Sugar Transport in Plants. *Rev. Mod. Phys.* **2016**, *88* (3). DOI: 10.1103/RevModPhys.88.035007

(20) Ueki, S.; Citovsky, V. The Systemic Movement of a Tobamovirus Is Inhibited by a Cadmiumion-Induced Glycine-Rich Protein. *Nat. Cell Biol.* **2002**, *4* (7), 478−485.

(21) Voigt, C. A. Callose-Mediated Resistance to Pathogenic Intruders in Plant Defense-Related Papillae. *Front. Plant Sci.* **2014**, *5*, 168.

(22) Kühn, C.; Franceschi, V. R.; Schulz, A.; Lemoine, R.; Frommer, W. B. Macromolecular Trafficking Indicated by Localization and Turnover of Sucrose Transporters in Enucleate Sieve Elements. *Science (Washington, DC, U. S.)* **1997**, *275*, 1298−1300.

(23) Ma, Y.; He, X.; Zhang, P.; Zhang, Z.; Ding, Y.; Zhang, J.; Wang, G.; Xie, C.; Luo, W.; Zhang, J. Xylem and Phloem Based Transport of CeO2 Nanoparticles in Hydroponic Cucumber Plants. *Environ. Sci. Technol.* **2017**, *51* (9), 5215−5221.
(24) Wang, Z.; Xie, X.; Zhao, J.; Liu, X.; Feng, W.; White, J. C.; Xing, B. Xylem-and Phloem-Based Transport of CuO Nanoparticles in Maize (Zea Mays L.). *Environ. Sci. Technol.* **2012**, *46*, 8.
(25) Milne, R. J.; Grof, C. P.; Patrick, J. W. Mechanisms of Phloem Unloading: Shaped by Cellular Pathways, Their Conductances and Sink Function. *Current Opinion in Plant Biology*. Elsevier Ltd June 1, 2018; pp 8−15.
(26) Lew, T. T. S.; Wong, M. H.; Kwak, S. Y.; Sinclair, R.; Koman, V. B.; Strano, M. S. Rational Design Principles for the Transport and Subcellular Distribution of Nanomaterials into Plant Protoplasts. *Small* **2018**, *14* (44), 1−13.
(27) Zhu, Z. J.; Wang, H.; Yan, B.; Zheng, H.; Jiang, Y.; Miranda, O. R.; Rotello, V. M.; Xing, B.; Vachet, R. W. Effect of Surface Charge on the Uptake and Distribution of Gold Nanoparticles in Four Plant Species. *Environ. Sci. Technol.* **2012**, *46* (22), 12391−12398.
(28) Shakiba, S.; Astete, C. E.; Paudel, S.; Sabliov, C. M.; Rodrigues, D. F.; Louie, S. M. Emerging Investigator Series: Polymeric Nanocarriers for Agricultural Applications: Synthesis, Characterization, and Environmental and Biological Interactions. *Environmental Science: Nano.*; Royal Society of Chemistry January 1, 2020; pp 37−67.
(29) Li, S.; Chung, H. S.; Simakova, A.; Wang, Z.; Park, S.; Fu, L.; Cohen-Karni, D.; Averick, S.; Matyjaszewski, K. Biocompatible Polymeric Analogues of DMSO Prepared by Atom Transfer Radical Polymerization. 2017.
(30) Yan, J.; Li, S.; Cartieri, F.; Wang, Z.; Hitchens, T. K.; Leonardo, J.; Averick, S. E.; Matyjaszewski, K. Iron Oxide Nanoparticles with Grafted Polymeric Analogue of Dimethyl Sulfoxide as Potential Magnetic Resonance Imaging Contrast Agents. *ACS Appl. Mater. Interfaces* **2018**, *10* (26), 21901−21908.
(31) Pang, X.; Zhao, L.; Akinc, M.; Kim, J. K.; Lin, Z. Novel Amphiphilic Multi-Arm, Star-like Block Copolymers as Unimolecular Micelles. *Macromolecules* **2011**, *44* (10), 3746−3752.
(32) Matyjaszewski, K. Atom Transfer Radical Polymerization (ATRP): Current Status and Future Perspectives. *Macromolecules* **2012**, *45* (10), 4015−4039.
(33) Lohaus, G.; Pennewiss, K.; Sattelmacher, B.; Hussmann, M.; Hermann Muehling, K. Is the Infiltration-Centrifugation Technique Appropriate for the Isolation of Apoplastic Fluid? A Critical Evaluation with Different Plant Species. *Physiol. Plant.* **2001**, *111* (4), 457−465.
(34) Guan, X.; Gao, X.; Avellan, A.; Spielman-Sun, E.; Xu, J.; Laughton, S.; Yun, J.; Zhang, Y.; Bland, G. D.; Zhang, Y. CuO Nanoparticles Alter the Rhizospheric Bacterial Community and Local Nitrogen Cycling for Wheat Grown in a Calcareous Soil. *Environ. Sci. Technol.* **2020**, *54* (14), 8699−8709.
(35) Kim, B. S.; Gao, H.; Argun, A. A.; Matyjaszewski, K.; Hammond, P. T. All-Star Polymer Multilayers as PH-Responsive Nanofilms. *Macromolecules* **2009**, *42* (1), 368−375.
(36) Lee, H.; Boyce, J. R.; Nese, A.; Sheiko, S. S.; Matyjaszewski, K. PH-Induced Conformational Changes of Loosely Grafted Molecular Brushes Containing Poly(Acrylic Acid) Side Chains. *Polymer* **2008**, *49* (25), 5490−5496.
(37) Wang, P.; Lombi, E.; Zhao, F. J.; Kopittke, P. M. Nanotechnology: A New Opportunity in Plant Sciences. *Trends in Plant Science*. Elsevier Ltd August 1, 2016; pp 699−712.
(38) Fujino, T.; Itoh, T. *Changes in Pectin Structure during Epidermal Cell Elongation in Pea (Pisum Sativum) and Its Implications for Cell Wall Architecture*; 1998; Vol. *39*.
(39) Lalonde, S.; Tegeder, M.; Throne-Holst, M.; Frommer, W. B.; Patrick, J. W. Phloem Loading and Unloading of Sugars and Amino Acids. *Plant, Cell and Environment*. John Wiley & Sons, Ltd January 1, 2003; pp 37−56.
(40) Avellan, A.; Yun, J.; Morais, B. P.; Clement, E. T.; Rodrigues, S. M.; Lowry, G. V. Critical Review: Role of Inorganic Nanoparticle Properties on Their 2 Foliar Uptake and in Planta Translocation. *Environ. Sci. Technol.* **2021**, DOI: 10.1021/acs.est.1c00178.
(41) Tegeder, M.; Hammes, U. Z. The Way out and in: Phloem Loading and Unloading of Amino Acids. *Current Opinion in Plant Biology*. Elsevier Ltd June 1, 2018; pp 16−21.
(42) Raliya, R.; Franke, C.; Chavalmane, S.; Nair, R.; Reed, N.; Biswas, P. Quantitative Understanding of Nanoparticle Uptake in Watermelon Plants. *Front. Plant Sci.* **2016**, *7*, 1288.
(43) Zhang, Z.; He, X.; Zhang, H.; Ma, Y.; Zhang, P.; Ding, Y.; Zhao, Y. Uptake and Distribution of Ceria Nanoparticles in Cucumber Plants. *Metallomics* **2011**, *3* (8), 816.
(44) Schwab, F.; Zhai, G.; Kern, M.; Turner, A.; Schnoor, J. L.; Wiesner, M. R. Barriers, Pathways and Processes for Uptake, Translocation and Accumulation of Nanomaterials in Plants - Critical Review. *Nanotoxicology* **2016**, *10* (3), 257−278.
(45) Wong, M. H.; Misra, R. P.; Giraldo, J. P.; Kwak, S. Y.; Son, Y.; Landry, M. P.; Swan, J. W.; Blankschtein, D.; Strano, M. S. Lipid Exchange Envelope Penetration (LEEP) of Nanoparticles for Plant Engineering: A Universal Localization Mechanism. *Nano Lett.* **2016**, *16* (2), 1161−1172.
(46) Ueki, S.; Citovsky, V. *Proc. Natl. Acad. Sci. U. S. A.* **2005**, *102*, 12089.
(47) Liu, X.; Wu, F.; Tian, Y.; Wu, M.; Zhou, Q.; Jiang, S.; Niu, Z. Size Dependent Cellular Uptake of Rod-like Bionanoparticles with Different Aspect Ratios. *Sci. Rep.* **2016**.
(48) Sousa, A. I.; Caçador, I.; Lillebø, A. I.; Pardal, M. A. Heavy Metal Accumulation in Halimione Portulacoides: Intra- and Extra-Cellular Metal Binding Sites. *Chemosphere* **2008**, *70* (5), 850−857.
(49) Orbovic'1, V.; Orbovic'1, O.; Achor, D.; Syvertsen, J. P. *Adjuvants Affect Penetration of Copper Through Isolated Cuticles of Citrus Leaves and Fruit*; 2007; Vol. *42*.
(50) Yeats, T. H.; Rose, J. K. C. The Formation and Function of Plant Cuticles. *Plant Physiol.* **2013**, *163*, 5−20.
(51) Spielman-Sun, E.; Avellan, A.; Bland, G. D.; Clement, E. T.; Tappero, R. V.; Acerbo, A. S.; Lowry, G. V. Protein Coating Composition Targets Nanoparticles to Leaf Stomata and Trichomes. *Nanoscale* **2020**, *12* (6), 3630−3636.
(52) Li, C.; Wang, P.; Lombi, E.; Cheng, M.; Tang, C.; Howard, D. L.; Menzies, N. W.; Kopittke, P. M. Absorption of Foliar-Applied Zn Fertilizers by Trichomes in Soybean and Tomato. *J. Exp. Bot.* **2018**.
(53) Borgatta, J. R.; Lochbaum, C. A.; Elmer, W. H.; White, J. C.; Pedersen, J. A.; Hamers, R. J. Biomolecular Corona Formation on CuO Nanoparticles in Plant Xylem Fluid. *Environ. Sci.: Nano* **2021**, *8* (4), 1067.